

# $\Lambda\Lambda$ Interaction and Neutron Stars

Yeunhwan Lim,<sup>1,\*</sup> Chang Ho Hyun,<sup>2,†</sup> Kyujin Kwak,<sup>3,‡</sup> and Chang-Hwan Lee<sup>4,§</sup>

<sup>1</sup>*Rare Isotope Science Project, Institute for Basic Science,  
Daejeon 305-811, Republic of Korea*

<sup>2</sup>*Department of Physics Education, Daegu University,  
Gyeongsan 712-714, Republic of Korea*

<sup>3</sup>*School of Natural Science, Ulsan National Institute of Science  
and Technology (UNIST), Ulsan 689-798, Republic of Korea*

<sup>4</sup>*Department of Physics, Pusan National University, Busan 609-735, Republic of Korea*

(Dated: November 18, 2014)

## Abstract

We investigate the effect of the  $\Lambda\Lambda$  interactions on the bulk properties of neutron star (NS). We employ a few Skyrme-type models and a finite-range force model in order to describe the  $\Lambda\Lambda$  interactions for the nuclear matter of NS. With the model parameters that reproduce the binding energies of the double- $\Lambda$  hypernuclei, we calculate the equation of state (EoS) for the matter of NS self-consistently. By solving the Tolman-Oppenheimer-Volkoff equation with the new EoS, we find that the bulk properties of NS, such as mass and radius, strongly depend on the  $\Lambda\Lambda$  interactions. It has been generally known (as “hyperonization puzzle”) that the existence of hyperons in NS matter is not well supported by the recent discovery of the high mass NS ( $M_{NS} \approx 2M_{\odot}$ ) because hyperons make the EoS soft. However, we find that some of our NS models can predict both the existence of the  $\sim 2M_{\odot}$  NS and the observationally constrained mass-radius relations. Our results indicate that the  $\Lambda\Lambda$  interactions could provide a clue to this puzzle.

PACS numbers: 97.60.Jd, 14.20.Jn

---

\*Electronic address: [yylim9057@ibs.re.kr](mailto:yylim9057@ibs.re.kr)

†Electronic address: [hch@daegu.ac.kr](mailto:hch@daegu.ac.kr)

‡Electronic address: [kkwak@unist.ac.kr](mailto:kkwak@unist.ac.kr)

§Electronic address: [cleee@pusan.ac.kr](mailto:cleee@pusan.ac.kr)

## I. INTRODUCTION

The existence of a neutron star (NS) has been observationally confirmed and the measured mass and radius of neutron stars have been used to partially constrain the physical properties of the dense nuclear matter. So far, about 70 NS have been observed and their distribution in mass has been accumulated according to their binary types [1]. In the X-ray/optical binaries, the mean and error-weighted mean of NS mass distribution are  $1.568M_{\odot}$  and  $1.368M_{\odot}$ , respectively, which implies that the measurement errors are relatively large. The NS-white dwarf binaries have similar precision in the mass distribution to that of the X-ray/optical binaries; the mean and error-weighted mean are  $1.543M_{\odot}$  and  $1.369M_{\odot}$ , respectively. On the other hand, the NS-NS binaries show relatively stable statistics; the mean and error-weighted mean are  $1.322M_{\odot}$  and  $1.402M_{\odot}$ , respectively. In all of these binaries, the mean masses do not exceed  $1.6M_{\odot}$ , and one may conclude that most of NS masses lie in the range of  $1.2M_{\odot} - 1.6M_{\odot}$ , which can be regarded as a canonical range of NS masses. Note that NS with larger masses have relatively larger measurement errors except for a few exceptions for the large NS masses, which were measured with high accuracy, e.g., PSR J1614-2230,  $(1.97 \pm 0.04)M_{\odot}$  [2] and PSR J0348+0432,  $(2.01 \pm 0.04)M_{\odot}$  [3].

By solving the Tolman-Oppenheimer-Volkoff (TOV) equation, one can see that the NS with large mass can have a high-density region in the core, providing a room for the existence of non-nucleonic degrees of freedom such as hyperons, Bose-Einstein condensation, free quark phase and etc. These exotic states relieve the pressure exerted by the Fermionic nature of nucleons, make the equation of state (EoS) soft, and eventually reduce the mass of NS. Among diverse possibilities, hyperons have been playing a key role in reducing the maximum mass of NS to the canonical range. However, recent observations of NS with  $(1.97 \pm 0.04)M_{\odot}$  and  $(2.01 \pm 0.04)M_{\odot}$  initiate a challenge to the existence of hyperons at the core of NS (so called “hyperonization puzzle”).

In order to solve the hyperonization puzzle, some studies based upon both relativistic and non-relativistic mean field (RMF and NRMF, respectively) models have been conducted so far. In fact, because of successful phenomenological description of stable nuclei, the RMF and NRMF models have been exclusively and intensively adopted in the study of NS, and hundreds of RMF and NRMF models have been suggested to date. The modern version of these models shows great accuracy in reproducing the properties of known nuclei. However,

the maximum mass of NS calculated with these models shows drastic fluctuations, ranging from  $1.4M_{\odot}$  to  $2.8M_{\odot}$  even without including any hyperon yet [4]. Main uncertainty comes from the extrapolation of models to the high density where no experimental data available. Therefore, the measurement of the  $\sim 2M_{\odot}$  NS from PSR J1614-2230 and PSR J0348+0432 can rule out some of RMF or NRMF models that predict the maximum mass less than  $2M_{\odot}$ .

When the effect of hyperons is included in the RMF models, the coupling constants of hyperons are fitted to the depth of hyperon-nucleus optical potentials at the nuclear saturation density in most of the RMF models. (Note that the hyperon-nucleus optical potentials are obtained from the single-strangeness hypernuclei.) With this method, the RMF models show the similar effect of hyperons on NS mass regardless of the differences among various RMF models; the mass of NS is depending on the background nuclear models [5]. In order to solve the hyperonization puzzle, some recent works introduced a repulsion that is caused by the vector-meson exchange in the RMF models [6]. In Ref. [7], by assuming a hard core of hyperons, one of the authors (CHH) obtained the maximum mass of NS close to  $2M_{\odot}$ . However, the parameterization used in these approaches is not directly compatible with hypernuclear data and relies partly on the theoretical arguments. Dealing with the interactions between hyperons is in a worse situation because there are not statistically sufficient data from the double-hypernuclei experiments against which the theoretical calculations are tested. In most cases, the coupling constants between hyperons are determined from the symmetry arguments. The coupling constants obtained in this manner show a very minor effect on the mass of NS [8–10], so in many works the interactions between hyperons are justified to be omitted for simplicity.

The purpose of this work is to explore the effect of the  $\Lambda\Lambda$  interactions on the EoS and the resulting bulk properties of NS on a “realistic” ground, in order to solve the hyperonization puzzle. By “realistic”, we mean that, rather than fixing the coupling constants of the  $\Lambda\Lambda$  interactions based upon the symmetry arguments as in the previous studies, we use both a few Skyrme-type models and a finite-range model that reproduce the empirical binding energies of the double- $\Lambda$  hypernuclei. For the nucleon and single- $\Lambda$  interactions and the nucleon-nucleon interactions, we also use the Skyrme-type models that are consistent with the experimental data. We find that our results with this “realistic modeling” turn out to be quite different from those of the RMF models, suggesting a possible solution to the hyperonization puzzle. We find that some of our models both predict the maximum mass of

$2M_\odot$  and are in good agreement with the observationally-constrained mass-radius relation [12].

We organize this paper as follows. Sect. II explains the Skyrme-type models for the nucleon-nucleon ( $NN$ ) interactions and the nucleon- $\Lambda$  ( $N\Lambda$ ) interactions. As mentioned above, we use both the Skyrme-type models and a finite-range force model for the  $\Lambda\Lambda$  interactions. Sect. II also contains some details of these models. Sect. III is devoted to the results about the properties of NS matter, and the consequent mass-radius relation of NS. We summarize our work and give some discussions in Sect. IV.

## II. INTERACTIONS

We employ the standard Skyrme-type forces for the  $NN$  interactions given in the form

$$\begin{aligned} v_{NN}(\mathbf{r}_{ij}) = & t_0(1 + x_0 P_\sigma) \delta(\mathbf{r}_{ij}) + \frac{1}{2} t_1 (1 + x_1 P_\sigma) [\mathbf{k}_{ij}^2 \delta(\mathbf{r}_{ij}) + \delta(\mathbf{r}_{ij}) \mathbf{k}_{ij}^2] \\ & + t_2 (1 + x_2 P_\sigma) \mathbf{k}_{ij} \cdot \delta(\mathbf{r}_{ij}) \mathbf{k}_{ij} + \frac{1}{6} t_3 (1 + x_3 P_\sigma) \rho_N^\epsilon(\mathbf{R}) \delta(\mathbf{r}_{ij}) \\ & + i W_0 \mathbf{k}_{ij} \cdot \delta(\mathbf{r}_{ij}) (\boldsymbol{\sigma}_i + \boldsymbol{\sigma}_j) \times \mathbf{k}_{ij}, \end{aligned} \quad (1)$$

where  $\mathbf{r}_{ij} = \mathbf{r}_i - \mathbf{r}_j$ ,  $\mathbf{R} = (\mathbf{r}_i + \mathbf{r}_j)/2$ ,  $\mathbf{k}_{ij} = -i(\nabla_i - \nabla_j)/2$ , the spin exchange operator  $P_\sigma = (1 + \boldsymbol{\sigma}_i \cdot \boldsymbol{\sigma}_j)/2$ , and the nucleon density  $\rho_N = \rho_n + \rho_p$ . We choose three models SLy4, SkI4, and SGI for the parameters of  $NN$  interactions. As shown in Ref. [11], these models are in reasonable agreement with the mass-radius constraints of the observed NS presented in Ref. [12]. The basic properties of the models are summarized in Table I. We note that the models also satisfy the maximum mass constraints given by PSR J1614-2230 or PSR J0348+0432.

The Skyrme-type interaction of a  $\Lambda$  hyperon in the nuclear medium was first proposed in Ref. [13], and later a phenomenological three-body term was added in Ref. [14]. The potential for the  $N\Lambda$  interaction in our work takes the form

$$\begin{aligned} v_{N\Lambda} = & u_0(1 + y_0 P_\sigma) \delta(\mathbf{r}_{N\Lambda}) + \frac{1}{2} u_1 [\mathbf{k}_{N\Lambda}^2 \delta(\mathbf{r}_{N\Lambda}) + \delta(\mathbf{r}_{N\Lambda}) \mathbf{k}_{N\Lambda}^2] \\ & + u_2 \mathbf{k}_{N\Lambda} \cdot \delta(\mathbf{r}_{N\Lambda}) \mathbf{k}_{N\Lambda} + \frac{3}{8} u'_3 (1 + y_3 P_\sigma) \rho_N^\gamma \left( \frac{\mathbf{r}_N + \mathbf{r}_\Lambda}{2} \right) \delta(\mathbf{r}_{N\Lambda}), \end{aligned} \quad (2)$$

where definitions of  $\mathbf{r}_{N\Lambda}$  and  $\mathbf{k}_{N\Lambda}$  follow the same convention as in the  $NN$  interaction. There are several parameter sets for the coupling constants in the  $N\Lambda$  potential [14–17]. We

$NN$ model	$\rho_0$	$B$	$S_v$	$L$	$K$	$m_N^*/m_N$	$M_{\max}/M_\odot$
SLy4	0.160	16.0	32.0	45.9	230	0.694	2.06
SkI4	0.160	16.0	29.5	60.4	248	0.649	2.19
SGI	0.155	15.9	28.3	63.9	262	0.608	2.25

TABLE I: Nuclear matter properties and the maximum mass of NS calculated from the  $NN$  Skyrme force models.  $\rho_0$ : saturation density in unit of  $\text{fm}^{-3}$ ,  $B$ : binding energy of the symmetric nuclear matter in unit of MeV,  $S_v$ : symmetry energy at the saturation density in unit of MeV,  $L$ : slope of the symmetry energy at the saturation density in unit of MeV,  $K$ : compression modulus of the symmetric matter at the saturation density in unit of MeV,  $m_N^*/m_N$ : ratio of the effective mass of the nucleon at the saturation density ( $m_N^*$ ) to the free mass of the nucleon ( $m_N$ ), and  $M_{\max}/M_\odot$ : maximum mass of NS in unit of the solar mass ( $M_\odot$ ).

$N\Lambda$ model	$\gamma$	$u_0$	$u_1$	$u_2$	$u'_3$	$y_0$	$y_3$	$U_\Lambda^{\text{opt}}$
HP $\Lambda$ 2	1	-399.946	83.426	11.455	2046.818	-0.486	-0.660	-31.23
OA2	1/3	-417.7593	1.5460	-3.2671	1102.2221	-0.3854	-0.5645	-28.27
YBZ6	1	-372.2	100.4	79.60	2000.	-0.107	0.	-29.73

TABLE II: Parameters for the  $N\Lambda$  interactions.  $u_0$  is in unit of  $\text{MeV} \cdot \text{fm}^3$ ,  $u_1$  and  $u_2$  in unit of  $\text{MeV} \cdot \text{fm}^5$ , and  $u'_3$  in unit of  $\text{MeV} \cdot \text{fm}^{3+3\gamma}$ .  $y_0$  and  $y_3$  are dimensionless. The last column  $U_\Lambda^{\text{opt}}$  is the depth of the  $\Lambda$ -nucleus optical potential in unit of MeV at the saturation density.

adopt the parameters from an old model, YBZ6 in Ref. [15] and the most recent ones, HP $\Lambda$ 2 and OA2 in Ref. [17]. Table II shows the parameters we use for the  $N\Lambda$  interactions.

For the interactions between  $\Lambda$  hyperons, a Skyrme-type force in the standard form was proposed in Ref. [18], where three sets of model parameters, S $\Lambda\Lambda$ 1, S $\Lambda\Lambda$ 2, and S $\Lambda\Lambda$ 3 were obtained from the fit to the binding energy  $B_{\Lambda\Lambda}$  of a double- $\Lambda$  hypernucleus  $^{13}_{\Lambda\Lambda}\text{B}$ . Recently new parameters have been obtained by considering the fission barrier of the actinide nuclei with two  $\Lambda$  hyperons [19], and the models we take into account in this work are labeled as S $\Lambda\Lambda$ 1' and S $\Lambda\Lambda$ 3'. The Skyrme-type force is written as

$$v_{\Lambda\Lambda}(\mathbf{r}_{ij}) = \lambda_0 \delta(\mathbf{r}_{ij}) + \frac{1}{2} \lambda_1 [\mathbf{k}_{ij}^2 \delta(\mathbf{r}_{ij}) + \delta(\mathbf{r}_{ij}) \mathbf{k}_{ij}^2] + \lambda_2 \mathbf{k}_{ij} \cdot \delta(\mathbf{r}_{ij}) \mathbf{k}_{ij} + \lambda_3 \rho_N^\alpha(\mathbf{R}) \delta(\mathbf{r}_{ij}), \quad (3)$$

$\Lambda\Lambda$ model	$\lambda_0$	$\lambda_1$	$\lambda_2$	$\lambda_3$	$\alpha$
S $\Lambda\Lambda$ 1	-312.6	57.5	0	0	-
S $\Lambda\Lambda$ 2	-437.7	240.7	0	0	-
S $\Lambda\Lambda$ 3	-831.8	922.9	0	0	-
S $\Lambda\Lambda$ 1'	-37.9	14.1	0	0	-
S $\Lambda\Lambda$ 3'	-156.4	347.2	0	0	-

TABLE III: Parameters of the  $\Lambda\Lambda$  interactions in the Skyrme-type force.  $\lambda_0$  is in unit of  $\text{MeV} \cdot \text{fm}^3$ , and  $\lambda_1$  in unit of  $\text{MeV} \cdot \text{fm}^5$ . Notice that all models considered here do not have  $\lambda_2$  momentum interaction and  $\lambda_3$ ,  $\alpha$  density dependent interaction.

Nuclei	$B_{\Lambda\Lambda}(\text{S}\Lambda\Lambda 1)$	$B_{\Lambda\Lambda}(\text{S}\Lambda\Lambda 2)$	$B_{\Lambda\Lambda}(\text{S}\Lambda\Lambda 3)$	$B_{\Lambda\Lambda}(\text{Exp.})$
${}^6_{\Lambda\Lambda}\text{He}$	11.88	9.25	7.60	$6.91 \pm 0.16$ [21]
${}^{10}_{\Lambda\Lambda}\text{Be}$	19.78	18.34	15.19	$14.94 \pm 0.13$ [22]
${}^{11}_{\Lambda\Lambda}\text{Be}$	20.55	19.26	16.27	$20.49 \pm 1.15$ [21]
${}^{12}_{\Lambda\Lambda}\text{Be}$	21.10	19.97	17.18	$22.23 \pm 1.15$ [21]
${}^{13}_{\Lambda\Lambda}\text{B}$	21.21	20.26	17.76	$23.30 \pm 0.70$ [21]

TABLE IV: Double  $\Lambda$  binding energies  $B_{\Lambda\Lambda}$  in unit of MeV calculated from theory [20] and measured from experiments [21, 22]. The SLy4 and HPA2 models are used for the  $NN$  interaction and the  $N\Lambda$  interaction, respectively. The results with S $\Lambda\Lambda$ 1' and S $\Lambda\Lambda$ 3' are not presented because they are not available.

and the model parameters are shown in Table III. Table IV shows the  $\Lambda\Lambda$  binding energy  $B_{\Lambda\Lambda}$  calculated with SLy4, HPA2, and three S $\Lambda\Lambda$  models [20].

In addition to the Skyrme-type force, we employ a finite-range force (FRF) model for the  $\Lambda\Lambda$  interaction as given in Ref. [23]. In this model, the potential is assumed in the form

$$v_{\Lambda\Lambda}^{\text{FRF}}(r) = \sum_{i=1}^3 (v_i + v_i^\sigma \boldsymbol{\sigma}_\Lambda \cdot \boldsymbol{\sigma}_\Lambda) e^{-\mu_i r^2}. \quad (4)$$

The model parameters in the potential are fixed in order to reproduce  $B_{\Lambda\Lambda}$  of  ${}^6_{\Lambda\Lambda}\text{He}$ , and their values are listed in Table IV of Ref. [23]. We use the same values for our calculations.

Because it is the first attempt to consider the non-Skyrme-type interactions in the frame-

work of the Skyrme-type models, it is necessary to address the motivation for such an attempt. The primary motivation is the fact that the predictions from the Skyrme-force models are not fully consistent with the experimental binding energies as shown in Table IV. For example, among the three SAA models, the SAA3 model predicts best the binding energy of  ${}^6_{\Lambda\Lambda}\text{He}$ , but its predicted values for the more massive nuclei deviate from the experimental values more severely than those predicted from the other two models. In contrast, the SAA1 model behaves in the opposite way. For this reason, we decide to consider the finite-range force model whose predictions are in reasonable agreement with the experimental values (Table V in Ref. [23]), although the applications of the finite-range force model were somehow limited. Furthermore, as mentioned in the introduction, the purpose of this work is to explore the effect of the  $\Lambda\Lambda$  interactions more broadly and precisely, in order to solve the hyperonization puzzle. Thus, it is worth considering as many models as possible that predict the experimental data consistently. Note that the hyperon-hyperon interactions in the RMF models are treated very naively, while several Skyrme-force models or few-body models, whose model parameters are adjusted explicitly to the experimental hypernuclear data, are available. Therefore, we believe that using these Skyrme-type force models or a finite-range force model is better to model the  $\Lambda\Lambda$  interactions in combination with the Skyrme-type models for the  $NN$  and  $NA$  interactions.

In general, when the  $\Lambda\Lambda$  interactions are introduced, the  $NA$  interactions are usually fitted first with the background  $NN$  interaction models, and then the  $\Lambda\Lambda$  interactions are added on top of the  $NN$  and  $NA$  interaction models. The model parameters of the  $NN$ ,  $NA$  and  $\Lambda\Lambda$  interactions determined in this way form a single complete set of the interaction model in consideration. In this respect, the way that we determine the model parameters in this work is not fully self-consistent because the SAA interaction models in Ref. [18] were determined with the SkM\* for the  $NN$  interaction and the YBZ5 for the  $NA$  interaction for the fitting of the  $\Lambda\Lambda$  potential parameters. However, this approach may be still valid because Table IV shows that the predicted binding energies are in relatively good agreement with the experimental data in spite of some partial mismatches in the interaction models. Furthermore, because it is generally known that the EoS of NS matter is not quite sensitive to the fine tuning to individual nuclei, the resulting mass-radius relation is not affected much by the details of the fitting procedure. For these reasons, we do not think that the inconsistency in the combined interactions that we used for this work will change the major

conclusions of the final results.

Once all the interactions are fixed, it is straightforward to calculate their matrix elements in the uniform infinite matter. The Hamiltonian density for nucleons is obtained as

$$\begin{aligned}
\mathcal{H}_N = & \sum_{i=n,p} \frac{\hbar^2}{2m_N} \tau_i + \rho_N (\tau_n + \tau_p) \left[ \frac{t_1}{4} \left( 1 + \frac{x_1}{2} \right) + \frac{t_2}{4} \left( 1 + \frac{x_2}{2} \right) \right] \\
& + \sum_{i=n,p} \tau_i \rho_i \left[ -\frac{t_1}{4} \left( 1 + \frac{x_1}{2} \right) + \frac{t_2}{4} \left( 1 + \frac{x_2}{2} \right) \right] \\
& + \frac{t_0}{2} \left[ \left( 1 + \frac{x_0}{2} \right) \rho_N^2 - \left( \frac{1}{2} + x_0 \right) (\rho_n^2 + \rho_p^2) \right] \\
& + \frac{t_3}{12} \left[ \left( 1 + \frac{x_3}{2} \right) \rho_N^2 - \left( \frac{1}{2} + x_3 \right) (\rho_n^2 + \rho_p^2) \right] \rho_N^\epsilon,
\end{aligned} \tag{5}$$

and the terms for  $\Lambda$  hyperon read

$$\begin{aligned}
\mathcal{H}_\Lambda = & \frac{\hbar^2}{2m_\Lambda} \tau_\Lambda + u_0 \left( 1 + \frac{1}{2} y_0 \right) \rho_N \rho_\Lambda + \frac{1}{4} (u_1 + u_2) (\tau_\Lambda \rho_N + \tau_N \rho_\Lambda) \\
& + \frac{3}{8} u'_3 \left( 1 + \frac{1}{2} y_3 \right) \rho_N^{\gamma+1} \rho_\Lambda + \mathcal{H}_{\Lambda\Lambda},
\end{aligned} \tag{6}$$

where  $\tau_N = \tau_n + \tau_p$ , and  $\mathcal{H}_{\Lambda\Lambda}$  stands for the term for the  $\Lambda\Lambda$  interactions. The Skyrme-type force results in

$$\mathcal{H}_{\Lambda\Lambda} = \frac{\lambda_0}{4} \rho_\Lambda^2 + \frac{1}{8} (\lambda_1 + 3\lambda_2) \rho_\Lambda \tau_\Lambda + \frac{\lambda_3}{4} \rho_\Lambda^2 \rho_N^\alpha, \tag{7}$$

and the finite-range force gives

$$\mathcal{H}_{\Lambda\Lambda}^{\text{FRF}} = \frac{1}{2} \sum_{i=1}^3 v_i \left( \frac{\pi}{\mu_i} \right)^{\frac{3}{2}} \rho_\Lambda^2 - \frac{1}{6\pi^4} \sum_{i=1}^3 (v_i + 3v_i^\sigma) (\pi \mu_i)^{\frac{3}{2}} F(x_i), \tag{8}$$

where  $x_i = k_F / \sqrt{\mu_i}$  and  $F(x) = e^{-x^2} (x^2 - 2) - (3x^2 - 2) + \sqrt{\pi} x^3 \text{erf}(x)$ . Here,  $k_F$  is the Fermi momentum and the error function,  $\text{erf}(x) = \frac{2}{\sqrt{\pi}} \int_0^x e^{-u^2} du$ .

### III. RESULTS

The total energy density ( $\mathcal{E} = \mathcal{E}_N + \mathcal{E}_\Lambda + \mathcal{E}_e + \mathcal{E}_\mu$ ) of the bulk matter can be obtained by minimizing the total Hamiltonian density ( $\mathcal{H} = \mathcal{H}_N + \mathcal{H}_\Lambda + \mathcal{H}_e + \mathcal{H}_\mu$ ) with the constraint of the charge neutrality condition, where  $\mathcal{E}_N$  and  $\mathcal{E}_\Lambda$  are evaluated from Eqs. (5, 6) and  $\mathcal{E}_e$  and  $\mathcal{E}_\mu$  can be found in Ref. [11]. Pressure is then calculated from the relation

$$P = \rho^2 \frac{\partial}{\partial \rho} \left( \frac{\mathcal{E}}{\rho} \right). \tag{9}$$



NS matter satisfies baryon number conservation, charge neutrality, and  $\beta$ -equilibrium, among which the second and third conditions read, respectively,

$$\rho_p = \rho_e + \rho_\mu, \quad (10)$$

and

$$\mu_n = \mu_p + \mu_e, \quad \mu_e = \mu_\mu, \quad \mu_n + m_n = \mu_\Lambda + m_\Lambda, \quad (11)$$

where the chemical potential is obtained from

$$\mu_i = \frac{\partial \mathcal{H}}{\partial \rho_i}. \quad (12)$$

By solving the above equations self-consistently, we can determine the EoS. Then, by plugging the EoS into the TOV equation, we obtain the maximum mass and the mass-radius relation of NS. Because our main focus is to solve the hyperonization puzzle which is related to the maximum mass, we first present the results of the maximum mass obtained from our selected models of the  $NN$ ,  $N\Lambda$ , and  $\Lambda\Lambda$  interactions. We find that some of our selected models can predict the observed maximum mass of  $\sim 2M_\odot$ , which provides a clue to solve the hyperonization puzzle. Because it is necessary to investigate these models in more detail, we also present the EoS and the  $\Lambda$  fraction obtained from these models. Finally, the mass-radius relation predicted from these models is compared with the observation.

### A. Maximum mass of NS

We present the maximum mass of NS for our selected models in Table V. In order to see the effect of the  $\Lambda$  hyperon, we considered three models for the  $N\Lambda$  interaction (HPA2, OA2, and YBZ6) and six models for the  $\Lambda\Lambda$  interaction. As expected, including only the  $N\Lambda$  interactions on top of the  $NN$  interactions reduces the maximum mass of NS significantly. It is also shown that the extent of the decrease in the maximum mass strongly depends on the choice of the  $N\Lambda$  interaction. For the same  $NN$  interaction model, the maximum mass is the smallest with the OA2 model, while it is the largest with the YBZ6 model. This implies that the relative stiffness of the  $N\Lambda$  interactions increases in the order of OA2, HPA2, and YBZ6. The decrease of the maximum mass due to the  $N\Lambda$  interaction ranges from  $0.4M_\odot$  to  $1.0M_\odot$ . Note that this range that we obtained is much wider than that predicted from the RMF models, which is  $0.2M_\odot - 0.5M_\odot$  (Ref. [5] and references therein). Our result

$NN$ model (without $\Lambda$ ) <sup>†</sup>	SLy4 (2.06)		SkI4 (2.19)			SGI (2.25)		
$N\Lambda$ model (no $\Lambda\Lambda$ ) <sup>††</sup>	HP $\Lambda$ 2* (1.51)	OA2 (1.08)	HP $\Lambda$ 2 (1.52)	OA2 (1.19)	YBZ6* (1.80)	HP $\Lambda$ 2 (1.52)	OA2 (1.22)	YBZ6* (1.79)
S $\Lambda\Lambda$ 1	<i>1.40</i>	1.00	1.41	1.12	<i>1.70</i>	1.42	1.16	<i>1.69</i>
S $\Lambda\Lambda$ 2	<i>1.58</i>	1.28	1.57	1.30	<i>1.79</i>	1.57	1.31	<i>1.77</i>
S $\Lambda\Lambda$ 3	<i>1.85</i>	1.57	1.87	1.62	<i>2.03</i>	1.88	1.65	<i>2.04</i>
S $\Lambda\Lambda$ 1'	<i>1.51</i>	1.08	1.51	1.18	<i>1.79</i>	1.51	1.21	<i>1.78</i>
S $\Lambda\Lambda$ 3'	<i>1.76</i>	1.43	1.76	1.47	<i>1.97</i>	1.77	1.49	<i>1.96</i>
FRF	<i>1.61</i>	1.22	1.60	1.25	<i>1.86</i>	1.59	1.26	<i>1.84</i>

<sup>†</sup> Maximum NS mass without both  $N\Lambda$  and  $\Lambda\Lambda$  interactions.

<sup>††</sup> Maximum NS mass with  $N\Lambda$  but without  $\Lambda\Lambda$  interactions.

TABLE V: Maximum mass of NS in units of solar mass with the  $NN$ ,  $N\Lambda$ , and  $\Lambda\Lambda$  interactions.

\* Numbers in italic correspond to three selected models, SLy4-HP $\Lambda$ 2, SkI4-YBZ6, and SGI-YBZ6, which give relatively large maximum NS mass.

(predicting a wider range of the decrease in the maximum mass) is very interesting because all the three  $N\Lambda$  models that we considered give very similar values for the optical potential depth at the saturation density (Table II). Without including the  $\Lambda\Lambda$  interaction, the OA2 model predicts too small values for the maximum mass regardless of the choice of the  $NN$  interaction models to be consistent with the lower limit of the canonical range of NS mass. Thus, the OA2 model may be ruled out in the case that the effect of the  $\Lambda$  hyperon is only the  $N\Lambda$  interaction. Note that the result for YBZ6 in combination with SLy4 is not presented because this case is not physically plausible. In this case,  $\mu_\Lambda$  is large and it also increases faster than  $\mu_n$ , making the chemical equilibrium between  $\Lambda$  and neutron unreachable, i.e., there is no solution to the third equation of Eq. (11). This may imply that the creation of hyperons in NS is possible only when the interplay between the  $NN$  and  $N\Lambda$  interactions is optimized.

Unlike the  $N\Lambda$  interactions that always reduce the maximum mass when they are included on top of the  $NN$  interactions, the  $\Lambda\Lambda$  interactions can both increase and decrease the maximum mass when they are included on top of the  $NN$  and  $N\Lambda$  interactions. However,

the effect of the  $\Lambda\Lambda$  interaction on the maximum mass varies with the selection of the model. The S $\Lambda\Lambda$ 1 and S $\Lambda\Lambda$ 1' models do not increase the maximum mass regardless of the  $NN$  and  $N\Lambda$  interaction models that we considered. In contrast, the S $\Lambda\Lambda$ 3, S $\Lambda\Lambda$ 3', and FRF models always increase the maximum mass with such a trend that the amount of mass increase from the  $N\Lambda$  value increases in the order of FRF, S $\Lambda\Lambda$ 3', and S $\Lambda\Lambda$ 3 for the given  $NN$  and  $N\Lambda$  interactions. Meanwhile, the S $\Lambda\Lambda$ 2 model either increases or decreases the maximum mass depending on the choice of the  $NN$  and  $N\Lambda$  interaction models. Note that the changes in the maximum mass from their  $N\Lambda$  values due to the inclusion of the various  $\Lambda\Lambda$  interactions in our consideration range from  $-0.1M_\odot$  to  $0.4M_\odot$ . This shows that the effect of the  $\Lambda\Lambda$  interactions on the maximum mass obtained from our calculations is larger than that obtained from the RMF models in which the  $\Lambda\Lambda$  interactions change the maximum mass from the  $N\Lambda$  values only by  $\pm 0.1M_\odot$  [8, 24].

The most important result that comes from Table V is that some of our models that combine the suitable  $NN$ ,  $N\Lambda$ , and  $\Lambda\Lambda$  interactions predict large values for the maximum mass of NS even though the hyperons are included. For example, the S $\Lambda\Lambda$ 3 and S $\Lambda\Lambda$ 3' models predict the recently observed maximum mass of NS,  $\sim 2M_\odot$ , when they are combined with the SkI4-YBZ6 and SGI-YBZ6 models. Because these models can provide a clue to solve the hyperonization puzzle, it is worth investigating these models in more detail. For this reason, we select some models from Table V which predict the large maximum mass only and present the EoS and the  $\Lambda$  fraction obtained from these models in the next two sections.

## B. Equation of state

Figure 1 shows the EoS of NS matter for the selected models that give large values for the maximum mass of NS. By considering the slopes in the plots, we can sort out the models into three kinds; S $\Lambda\Lambda$ 1 and S $\Lambda\Lambda$ 1' as soft, S $\Lambda\Lambda$ 2 and FRF as mild, and S $\Lambda\Lambda$ 3 and S $\Lambda\Lambda$ 3' as hard.

In general, models with stiffer EoS predict larger maximum mass and our results in Table V show that most of the models follow this general trend. However, an exception to this general trend seems to be seen in S $\Lambda\Lambda$ 2 in comparison with S $\Lambda\Lambda$ 1' and FRF, in particular when we consider the slopes of the EoS curves at high densities (correspond to

large  $\mathcal{E}$  in the plots). The EoS curve of SAA2 (dotted line) is much stiffer than that of SAA1' (dot-dashed line), especially at high densities, but the maximum mass predicted from SAA2 is just slightly larger or even smaller than that predicted from SAA1' . Similarly, FRF (orange dashed line) is softer than SAA2 also at high densities, but the maximum mass predicted from FRF is larger than that predicted from SAA2 for all three cases in consideration.

In order to understand this exceptional behavior between the EoS and the maximum mass seen in some models, we mark the locations corresponding to the center of NS with the maximum mass by filled circles on the EoS curves in Figure 1. First of all, the locations of filled circles vary significantly from model to model, which implies that NS having the maximum mass in each model has different energy density and pressure at the center. Note that the origin of the plot corresponds to the surface of NS and the EoS curve traces the interior of NS (as a function of radius) from the surface to the center corresponding to the filled circle. Roughly speaking, the maximum mass is obtained by integrating the energy density over the entire NS, more accurately over the radius of NS in 1D spherical coordinates. Therefore, the part of the EoS curve only between the origin and the filled circle is relevant to the calculation of the maximum mass. Having this in mind, we re-examine the three EoS curves of SAA2 , SAA1' , and FRF, and find that within the relevant part of the EoS curve, the stiffness-maximum mass trend is not violated severely. FRF is always stiffer than SAA2 at low densities, which is consistent with the results of the maximum mass, i.e., the maximum mass of FRF is always larger than that of SAA2 in all three cases in consideration. In case of SLy4+HPA2, the relevant EoS curve of SAA2 is extended to larger energy density than that of FRF, implying that the calculation of the maximum mass should include the contribution from the partial EoS curve of SAA2 between  $\mathcal{E} \approx 1600 \text{MeV} \cdot \text{fm}^{-3}$  and  $\mathcal{E} \approx 2200 \text{MeV} \cdot \text{fm}^{-3}$  in comparison with the relevant EoS curve of FRF. However, the contribution from this partial EoS curve of SAA2 to the maximum mass is not significant because it is so close to the center of the NS that it occupies only a small fraction of the total volume, i.e., of the total mass. In other words, in the SAA2 model, the energy density changes quite a lot near the center in comparison with the FRF model. Similarly, the EoS curve of SAA1' that is relevant to the calculation of the maximum mass is as steep as that of SAA2 , in particular at low energy densities (between  $\sim 500 \text{MeV} \cdot \text{fm}^{-3}$  and  $\sim 750 \text{MeV} \cdot \text{fm}^{-3}$ ) for the cases of SkI4+YBZ6 and SGI+YBZ6. Thus, the stiffness-maximum mass trend also holds between

	SLy4		SkI4			SGI		
	HPA2	OA2	HPA2	OA2	YBZ6	HPA2	OA2	YBZ6
$\rho_{\text{crit}}$	0.453	0.380	0.374	0.340	0.455	0.352	0.325	0.412
$M/M_{\odot}$	1.17	0.90	1.19	1.04	1.51	1.21	1.08	1.47

TABLE VI: The critical density  $\rho_{\text{crit}}$  in units of  $\text{fm}^{-3}$  and the corresponding mass of NS that has the central density equal to the critical density.

SAA1' and SAA2 .

A brief summary of this section is as follows. For all of our selected models that predict the large maximum mass, a general trend between the stiffness of the EoS and the maximum mass of NS (i.e., the stiffer the EoS, the larger the maximum mass) always holds. Because all of our selected models include all the interactions involving the  $\Lambda$  hyperons ( $NN$ ,  $N\Lambda$ , and  $\Lambda\Lambda$ ), we can say that the general trend holds even when the full effect of the  $\Lambda$  hyperons is included. The  $\Lambda$  hyperons affect the EoS in such a way that the more the  $\Lambda$  hyperons exist, the softer the EoS becomes. So, in the following section, we present the fraction of the  $\Lambda$  hyperons for the same set of our selected models.

### C. $\Lambda$ hyperon fraction

In Table VI, we list the critical density  $\rho_{\text{crit}}$  at which hyperons begin to appear in the interior of NS and the corresponding mass of NS in units of solar mass ( $M/M_{\odot}$ ) whose central density is  $\rho_{\text{crit}}$ . The critical density increases with the stiffness of the  $N\Lambda$  interaction, in such a way that  $\text{YBZ6} > \text{HPA2} > \text{OA2}$  for a given  $NN$  interaction. This tendency can be understood from Eq. (11); more repulsive  $N\Lambda$  interactions result in larger chemical potentials of  $\Lambda$  hyperons. In contrast, for a given  $N\Lambda$  interaction, the critical density decreases with the stiffness of the  $NN$  interaction (the  $NN$  interaction models get stiffer in the way that  $\text{SGI} > \text{SkI4} > \text{SLy4}$ ). This can also be understood from Eq. (11); more repulsive  $NN$  interactions result in large chemical potentials of nucleons ( $\mu_n$ ) and make the chemical equilibrium between nucleons and  $\Lambda$  hyperons reached at the lower density.

Figure 2 displays the fraction of  $\Lambda$  hyperons as a function of the total baryon number density for the same selected models for which the EoS was presented in Figure 1. Regardless

of the models, the  $\Lambda$  fraction behaves very similarly near the critical density, but depending on the  $\Lambda\Lambda$  interaction, it varies significantly as the total baryon number density increases. As in Figure 1, we mark the locations of the center of NS with the maximum mass by using filled circles in Figure 2. Note again that the part of the fraction curve after the filled circle (i.e., the fractions at the large total baryon densities) is not relevant to the calculation of the maximum mass. Up to the locations of the filled circles, models with smaller  $\Lambda$  fractions predict the larger maximum mass of NS. In particular, the particle fraction curves of SAA2, SAA1', and FRF (for which we discussed the general trend between the EoS and the maximum mass in more detail in the previous section) show distinctively the trend between the fraction and the maximum mass. The fraction of FRF is always smaller than that of SAA2 in the relevant part of the fraction curve, which is consistent with the trend of the maximum mass such that the maximum mass of FRF is always larger than that of SAA2. Between SAA2 and SAA1', the fraction curves of these two models cross each other before they reach the locations of filled circles, which implies that the fraction of  $\Lambda$  hyperons in SAA1' is very similar to that in SAA2 up to the locations of the filled circles in the sense of average (although the fraction curves of SAA1' are always above those of SAA2 at large total baryon densities).

Combining the two trends, one between the EoS and the maximum mass shown in Figure 1 and the other between the  $\Lambda$  fraction and the maximum mass shown in Figure 2, we can confirm the effect of  $\Lambda$  hyperons on the EoS; the more  $\Lambda$  hyperons exist inside NS, the softer the EoS becomes (thus making the maximum mass smaller). However, the discussions so far, which are based on the maximum mass, the EoS, and the  $\Lambda$  fractions, do not include any information on the size of NS which also constrains the model predictions together with the mass. In the next section, we present the mass-radius relation obtained from our selected models that predict the large maximum mass.

#### D. Mass-radius relation

Figure 3 shows the mass-radius relation of neutron stars for the selected models which were used to get the EoS and  $\Lambda$  fractions in Figures 1 and 2, respectively. Flat bands around  $2M_\odot$  mark the range  $(1.97 \pm 0.04)M_\odot$  and  $(2.01 \pm 0.04)M_\odot$ , masses of PSR J1614-2230 and PSR J0348+0432, respectively. Green and brown regions (color online) near the center of

each panel represent the mass-radius constraints obtained from statistical analysis of the observed NS in Ref. [12]. For simplicity, we call the former constraint PSR1614 and the latter SLB2010. The mass-radius relation justifies our selection of the three  $NN$  models, which are in reasonable agreement with both the PSR1614 and SLB2010 constraint. A slight deviation is seen in case of SGI, in which the mass-radius curve of SGI (the black solid line in the bottom panel of Figure 3) is outside the SLB2010 zone by about 0.5 km in the radius. However, under the large uncertainties in the observed size of NS, we believe that it is worth considering the models with the 0.5 km deviation in the radius such as SGI.

As expected, at the same radius, the  $\Lambda$  hyperons reduce the mass of NS in comparison with the case without them. This is shown in Figure 3. Furthermore, the reduction in the mass due to the  $\Lambda$  hyperons (from the case without them) decreases with the stiffness of the EoS. In other words, when the hyperons are included, the models with stiff EoS (such as SAA3) have larger mass than those with soft EoS (such as SAA1) at the same radius. However, even when the hyperons are included, the models in our consideration can still satisfy both the PSR1614 and SLB2010 constraint, which supports the conclusion that we drew for the hyperonization puzzle before; the maximum mass of  $\sim 2M_\odot$  is achievable even with the  $\Lambda$  hyperons included. The models that predict the maximum mass of  $\sim 2M_\odot$  are also in reasonable agreement with the mass-radius relation SLB2010, which puts an additional strong constraint on the models. Among our selected models, it is SAA3 and SAA3' in combination of SkI4+YBZ that satisfy both the PSR1614 and SLB2010 best. The other models satisfy only one of these two constraints.

#### IV. SUMMARY AND DISCUSSION

In this work, we try to solve the hyperonization puzzle, which has been stated as that hyperons appearing in NS are not able to predict NS with large mass, especially  $\sim 2M_\odot$ . In order to do this, we included the  $\Lambda\Lambda$  interactions on top of the  $NA$  and  $NN$  interactions. In the previous studies such as the RMF models, the interactions between  $\Lambda$  hyperons have been treated based upon the symmetry properties of quark models, thus the connection with the empirical data has not been so tight. Here, we employed more realistic  $\Lambda\Lambda$  interactions which are adjusted to various data such as single-particle energy levels, binding energies, bond energies, and etc. of known double- $\Lambda$  hypernuclei. We find that the employed  $\Lambda\Lambda$

interactions result in a wide variety of the maximum mass of NS, the EoS of NS matter, the  $\Lambda$  fractions inside NS, and the mass-radius relation. However, some models satisfy both the recent constraint on the maximum mass ( $\sim 2M_\odot$ ) and the mass-radius relation, which provides a clue to solve the hyperonization puzzle, i.e., the existence of hyperons inside NS can be still compatible with the large-mass NS, even up to  $\sim 2M_\odot$ .

An important point of this work is that the models we adopted for the  $NN$ ,  $N\Lambda$ , and  $\Lambda\Lambda$  interactions are consistent with the currently available nuclear and hypernuclear data, thus additional *ad hoc* assumptions or modification of the model parameters are not required in order to make the hyperon stars feasible. Note that uncertainties in the model predictions are primarily caused by fitting the model parameters to nuclear data with some uncertainties or just by lacking the sufficient data of double- $\Lambda$  hypernuclei. As an alternative approach, if we were to take into account the constraints from astronomical observations such as mass, mass-radius relation, and surface temperature of NS, we could possibly constrain the model parameters involved in the  $\Lambda$  hyperons and obtain a better understanding of the state of matter at supra-saturation densities. As an example of this approach, in Figure 4, we plot the maximum mass of NS for certain ranges of  $\lambda_2$  and  $\lambda_3$  values which are used for the Skyrme-type  $\Lambda\Lambda$  interaction models as in Table III. In this example, the combined model of SkI4 with HPA2 and SAA3 is used to see the behavior the maximum mass of NS when the variation of  $\lambda_2$  and  $\lambda_3$  are allowed. As seen in table V, the maximum mass of the model is only  $1.87M_\odot$  without the  $\lambda_2$  momentum interaction and  $\lambda_3$  density dependent manybody interaction. The maximum mass of NS, however, can reach up to  $2.0M_\odot$  if we consider repulsive  $\lambda_2$  and  $\lambda_3$ . This also suggests the clue for the hyperonization puzzle. When more abundant data for the double- $\Lambda$  hypernuclei are available, we may be able to determine the values of  $\lambda_2$  and  $\lambda_3$  from the data and to compare them with the observations of the NS.

As a final remark, we discuss some limitations of our present work. As mentioned before, the parameters of the  $N\Lambda$  and  $\Lambda\Lambda$  interactions are generally determined on top of a given  $NN$  interaction model, so the parameters of the whole interactions determined in this way form a unique set of an interaction model. On the other hand, our investigations are based on a hybrid scheme, in which we combine the  $NN$ ,  $N\Lambda$ , and  $\Lambda\Lambda$  interactions piece by piece among the different models. For this reason, errors can be generated by the lack of self-consistency. However, relevant works show that even the hybrid applications of these types of models can reproduce the hypernuclear phenomenology fairly well [14, 20]. As for the



work of NS, the models for the  $NN$  and  $N\Lambda$  interactions used in Ref. [25] are completely different from those we used in our present work. However, as long as the  $NN$  and  $N\Lambda$  interaction models predict similar values of the maximum mass, the maximum masses of NS calculated using the same  $\Lambda\Lambda$  interactions do not change significantly, depending on the choice of the  $NN$  and  $N\Lambda$  interactions.

Another limitation of our current work arises from the omission of  $\Sigma$  and  $\Xi$  hyperons. Present knowledge about the  $\Sigma$ -hypernuclei indicates that  $\Sigma$  feels repulsion when it is embedded in a nucleus, so the  $\beta$ -equilibrium condition for  $\Sigma$  hyperons can be met when the density is substantially high. As for the  $\Xi$  hyperon, because its rest mass is larger than that of  $\Lambda$  by about 200 MeV, if the attraction of  $\Xi$  were not much stronger than that of  $\Lambda$ ,  $\Lambda$  hyperons would be predominantly populated in NS matter. Though our investigation is not complete at this moment in the aspect of the self-consistent application of models and the full account of exotic degrees of freedom, we expect that these two effects are not large enough to alter the conclusion of this work. However, it is still worth continuing to investigate them in the future studies.

### Acknowledgments

YL was supported by the Rare Isotope Science Project funded by the Ministry of Science, ICT and Future Planning (MSIP) and National Research Foundation (NRF) of KOREA. CHH is grateful to the Institute for Basic Science, where part of the work was completed. KK was partly supported by the Korea Astronomy and Space Science Institute under the R&D program (Project No. 2013-1-600-01) supervised by the Ministry of Science, ICT and Future Planning (MSIP). CHL was supported by the Research Fund Program of Research Institute for Basic Sciences, Pusan National University, Korea, 2014, Project No. RIBS-PNU-2014-110.

- 
- [1] J. M. Lattimer, *Ann. Rev. Nucl. Part. Sci.* **62**, 485 (2012).
  - [2] P. Demorest, T. Pennucci, S. Ransom, M. Roberts, and J. W. T. Hessels, *Nature*, **467**, 1081 (2010).
  - [3] J. Antoniadis *et al.*, *Science* **340**, 448 (2013).

- [4] J. M. Lattimer and M. Prakash, Phys. Rev. Lett. **94**, 111101 (2005).
- [5] S. Weissenborn, D. Chatterjee, and J. Schaffner-Bielich, Phys. Rev. C **85**, 065802 (2012).
- [6] S. Weissenborn, D. Chatterjee, and J. Schaffner-Bielich, Nucl. Phys. A **914**, 421 (2013).
- [7] C. H. Hyun, Prof. Theor. Phys. Suppl. **168**, 627 (2007).
- [8] I. Bednarek, and R. Manka, J. Phys. G: Nucl. Part. Phys. **31**, 1009 (2005).
- [9] C. Y. Ryu, C. H. Hyun, S. W. Hong, and B. T. Kim, Phys. Rev. C **75**, 055804 (2007).
- [10] C. Y. Ryu, C. H. Hyun, and S. W. Hong, J. Korean Phys. Soc. **54**, 1448 (2009).
- [11] Y. Lim, C. H. Hyun, K. Kwak, and C.-H. Lee, Phys. Rev. C **89**, 055804 (2014).
- [12] A. W. Steiner, J. M. Lattimer, and E. F. Brown, ApJ **722**, 33 (2010).
- [13] M. Rayet, Nucl. Phys. A **368**, 381 (1981).
- [14] D. E. Lansky, and Y. Yamamoto, Phys. Rev. C **55**, 2330 (1997).
- [15] Y. Yamamoto, H. Bando, and J. Zofka, Prog. Theor. Phys. **80**, 757 (1988).
- [16] F. Fernandez, T. Lopez-Arias, and C. Prieto, Z. Phys. A **334**, 349 (1989).
- [17] N. Guleria, S. K. Dhiman, and R. Shyam, Nucl. Phys. A **886**, 71 (2012).
- [18] D. E. Lansky, Phys. Rev. C **58**, 3351 (1998).
- [19] F. Minato, and S. Chiba, Nucl. Phys. A **856**, 55 (2011).
- [20] N. Guleria, S. K. Dhiman, and R. Shyam, Int. J. Mod. Phys. E **23**, 1450026 (2014).
- [21] K. Nakazawa *et al.*, Nucl. Phys. A **835**, 207 (2010).
- [22] M. Danysz *et al.*, Nucl. Phys. **49**, 121 (1963).
- [23] E. Hiyama, M. Kamimura, T. Motoba, T. Yamada, and Y. Yamamoto, Phys. Rev. C **66**, 024007 (2002).
- [24] A.-J. Mi, and W. You, Commun. Theor. Phys. **53**, 133 (2010).
- [25] L. Mornas, Eur. Phys. J. A **24**, 293 (2005).

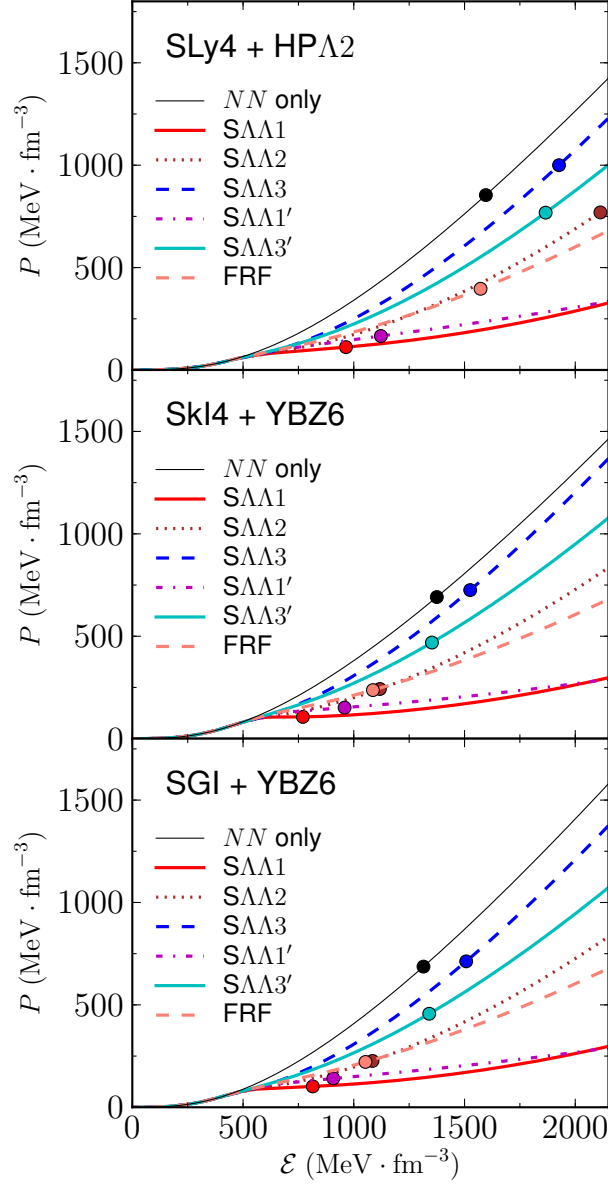


FIG. 1: (Color online) EoS for the selected models that predict the large maximum mass of NS. Different lines indicate the various  $\Lambda\Lambda$  interactions that we consider in this paper. For comparison, the EoS without any contribution from the  $\Lambda$  hyperon ( $NN$  only) is also plotted. Filled circles indicate the locations on the EoS curves corresponding to the center of NS with the maximum mass.

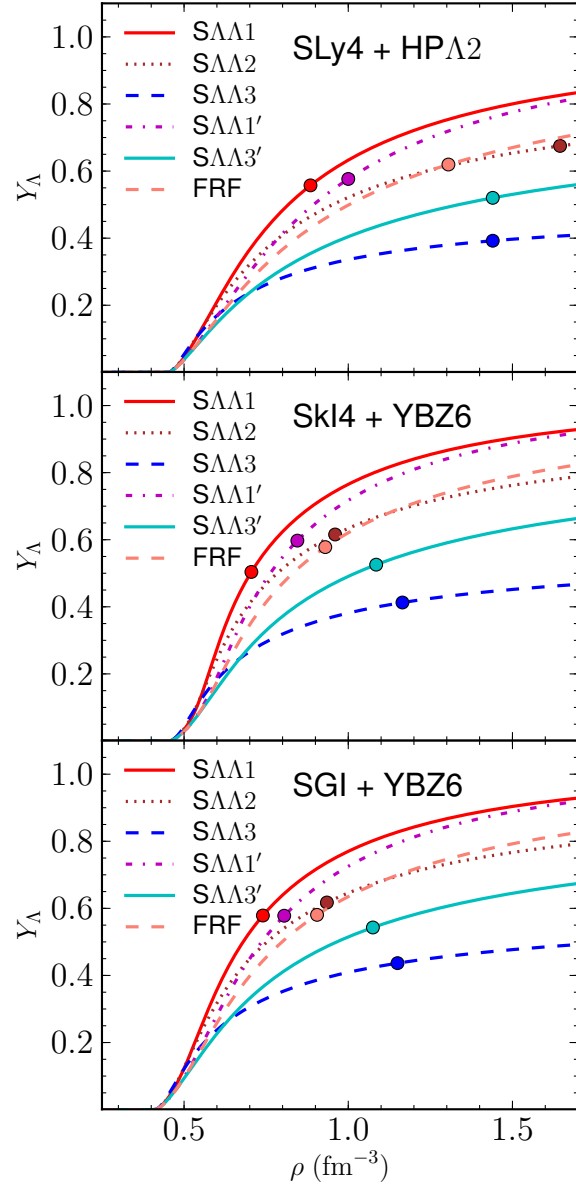


FIG. 2: (Color online) Particle fraction of  $\Lambda$  hyperons as a function of the total baryon number density. The  $\Lambda$  fraction ( $Y_\Lambda$ ) is defined as  $\rho_\Lambda/\rho$ , where  $\rho$  is the total baryon number density, i.e.,  $\rho = \rho_n + \rho_p + \rho_\Lambda$ .

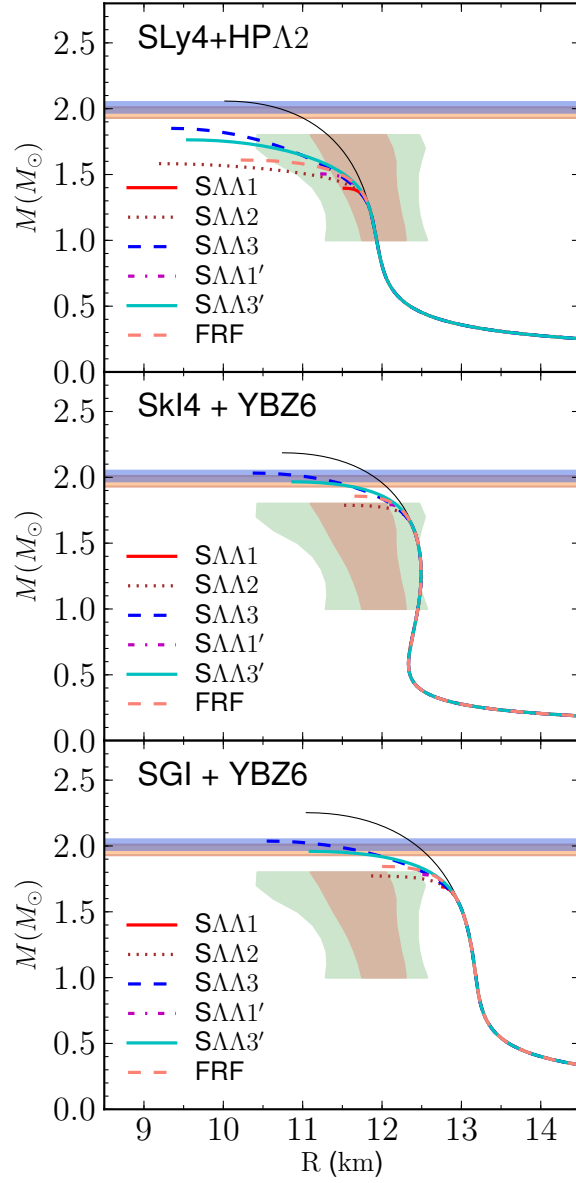


FIG. 3: (Color online) Mass-radius of neutron stars for the selected models. For comparison, the mass-radius relation without any contribution from  $\Lambda$  hyperons is also plotted as a black solid line in each panel. Two flat bands (with purple and orange color) denote the mass ranges of PSR J1614-2230 ( $1.97 \pm 0.04 M_\odot$ ) and PSR J0348+0432 ( $2.01 \pm 0.04 M_\odot$ ), respectively. Green and brown regions near the center are the mass-radius ranges obtained from Ref. [12].

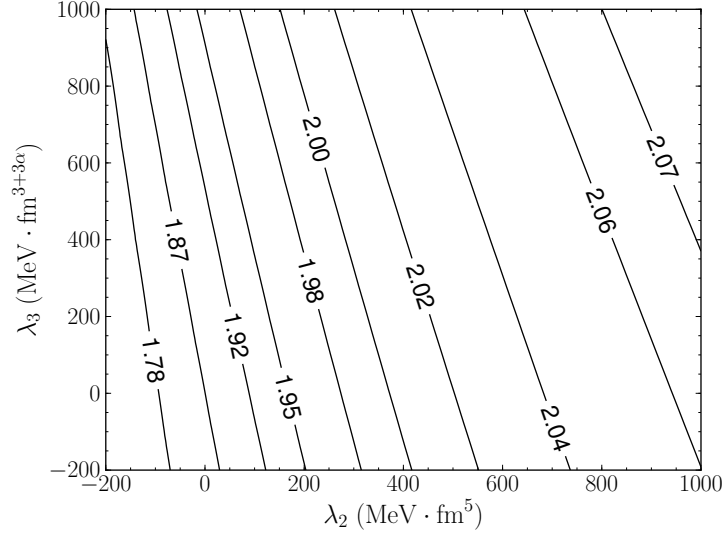


FIG. 4: Contour plot of the maximum mass of NS in units of solar mass as functions of  $\lambda_2$  and  $\lambda_3$  which are used in the Skyrme-type  $\Lambda\Lambda$  interaction models. Here,  $\alpha$  is fixed to  $1/3$  (see Table III). The  $NN$  and  $N\Lambda$  interactions are SkI4 and HPA2, respectively. For  $\Lambda\Lambda$  interaction, S $\Lambda\Lambda$ 3 is used.